An intranasal self-amplifying RNA SARS-CoV-2 vaccine produces durable respiratory and systemic immunity

Madeleine F. Jennewein[1], Samuel Beaver[1], Peter Battisti[1], Julie Bakken[1], Derek Hanson[1], Raodoh Mohamath[2], Jasneet Singh[1], Noah Cross[1], Sierra Reed[3], Alana Gerhardt[3], Corey Casper[1,2,3,4,5,6], Emily A. Voigt[1*]

[1]RNA Program, Access to Advanced Health Institute (AAHI), Seattle, WA 98102, USA

[2]Formulations, Access to Advanced Health Institute (AAHI), Seattle, WA 98102, USA

[3]Product Development and Characterization, Access to Advanced Health Institute (AAHI), Seattle, WA 98102, USA

[4]Department of Global Health, University of Washington, Seattle, WA 98195, USA

[5]Department of Medicine, University of Washington, Seattle, WA 98195, USA

[6]Vaccine and Infectious Disease Division, Fred Hutchinson Cancer Center, Seattle, WA 98109, USA

*Corresponding author: Emily A. Voigt, RNA Platform Team Lead, Access to Advanced Health Institute, 1616 Eastlake Ave E, Suite 400, Seattle, WA 98102; Phone: (206) 858-6108; Email: emily.voigt@aahi.org

Short title: An intranasal saRNA vaccine for SARS-CoV-2

Keywords: RNA, saRNA, self-amplifying RNA, nanostructured lipid carrier, thermostable, SARS-CoV-2, COVID-19, intranasal

Abstract

While mRNA vaccines have been highly effective over the past 2 years in combating severe acute respiratory syndrome coronavirus 2 (SARS-CoV-2), waning of vaccine-induced antibody responses and lack of induction of respiratory tract immunity contribute to ongoing infection and transmission. However, intranasally (i.n.) administered vaccines may induce mucosal immunity at the site of respiratory virus infection and may thus boost protection. In this work, we present an i.n. administered SARS-CoV-2 self-amplifying RNA (saRNA) vaccine, delivered by a nanostructured lipid carrier (NLC), which induces both potent respiratory mucosal and systemic immune responses. Following prime-boost immunization in C57BL/6 mice, i.n. vaccination induces serum neutralizing antibody titers, bone marrow resident IgG-secreting cells, and robust systemic polyfunctional T cells, similar to intramuscular (i.m.) vaccination. The intranasal vaccine additionally induces key SARS-CoV-2-reactive lung-resident polyfunctional memory and lung-homing T cell populations. As a booster following i.m. administration, the i.n. vaccine also elicits robust mucosal and systemic immunity, exceeding an i.m. booster, durable for at least 4 months. This i.n. saRNA vaccine's potent mucosal and systemic immunogenicity may be key for combating SARS-CoV-2 and other respiratory pathogens.

Introduction

The ongoing severe acute respiratory syndrome coronavirus 2 (SARS-CoV-2) pandemic has led to the rapid advancement and development of novel vaccines for coronavirus disease 2019 (COVID-19). Since their introduction in late 2020, two now FDA-approved mRNA vaccines (Comirnaty and Spikevax) have had a remarkable impact on the trajectory of the pandemic and were developed at unprecedented speeds [1]. However, while these vaccines have displayed remarkable efficacy at preventing severe COVID-19 and slowing the worldwide pandemic, the lack of vaccine-induced local immunity in the respiratory tract allows for mild infection despite vaccination, resulting in transmission by vaccinated people [2–4]. Between lack of vaccine

induction of mucosal immunity, newly emerging variants [5], waning efficacy of currently-approved mRNA vaccines [6], need for frequent booster doses [7], vaccine hesitancy in part fueled by a fear of needles [8], and limited access to cold chain storage [9], global susceptibility to SARS-CoV-2 remains high. Improved vaccines and associated technologies are therefore necessary to fully combat the epidemic.

Intranasally (i.n.) administered vaccines can provide protection from respiratory pathogens by stimulating mucosal immune responses [10], and may be key to providing sustained, potent immunity to SARS-CoV-2 and other respiratory pathogens. Unlike intramuscularly (i.m.) administered vaccines, i.n. vaccines demonstrate the induction of critical mucosal immune cells, generating mucosal IgA-secreting cells within the mucosa and respiratory tract as well as specific effector cell subsets, including tissue-resident memory (T_{RM}) T cells that are maintained within the lung [11–18]. Such mucosal immunity, mediated by IgA antibodies and lung-resident memory T cells, can prevent early-stage infection and viral replication and shedding, minimizing chances for viral transmission [12,13,18–20]. Effective i.n. vaccines can also induce cross-reactive antibodies and thus provide expanded protection to multiple strains [21]. Intranasal vaccination also presents many other advantages, such as easier needle-free administration, higher patient compliance, pediatric inclusion, and easier storage and transport [22], and thus potentially increased vaccine uptake. However, while several i.n. vaccines are currently under development for SARS-CoV-2, most of these rely on older vaccine technologies, i.e., live attenuated viruses and viral vectors [1], creating a slow pathway to manufacturing, testing, and licensing. Fortunately, bridging RNA vaccine technologies to i.n. delivery is possible, combining the production speed of RNA vaccines with the mucosal immune stimulation of i.n. vaccines.

We previously developed an i.m. administered nanostructured lipid carrier(NLC)-delivered self-amplifying RNA (saRNA) vaccine against SARS-CoV-2 [23,24], which induces both high serum neutralizing responses [25–27] and robust activation of $CD4^+$ and $CD8^+$ T cells, responses that may be critical to sustained potent immunity [26]. This saRNA-NLC vaccine platform additionally has unique thermostability relative to other mRNA delivery systems [24,28–30], and may be readily lyophilized and stored at room temperature for months or under refrigeration likely for years [24,30].

We now demonstrate that an i.n. administration of our saRNA SARS-CoV-2 vaccine strongly induces both systemic and mucosal immunity in preclinical models. Key mucosal lung-resident effector T cell populations, largely absent in the i.m. vaccine, are induced to high levels by the i.n. vaccine. We also demonstrate that this vaccine has great potential as a booster dose following i.m. immunization to elicit durable mucosal immunity. This i.n. saRNA-NLC vaccine candidate combines the speed and manufacturability of RNA vaccines with the potent immunogenicity of i.n. vaccines in a thermostable formulation that represents a significant new tool for current and future pandemic response.

Results

saRNA-NLC vaccine vector

The SARS-CoV-2 vaccine saRNA contains a codon-optimized Wuhan-strain D614G SARS-CoV-2 spike protein sequence driven by a Venezuelan equine encephalitis virus (VEEV)-based replicon (Figure 1A) [24]. This saRNA is complexed to the exterior of AAHI's proprietary NLC nanoparticle to create the final vaccine product AAHI-SC2 (Figure 1B). This construct is highly thermostable maintaining immunogenicity after storage at 25°C lyophilized for up to 2 months and at 4°C lyophilized for up to 10 months [24].

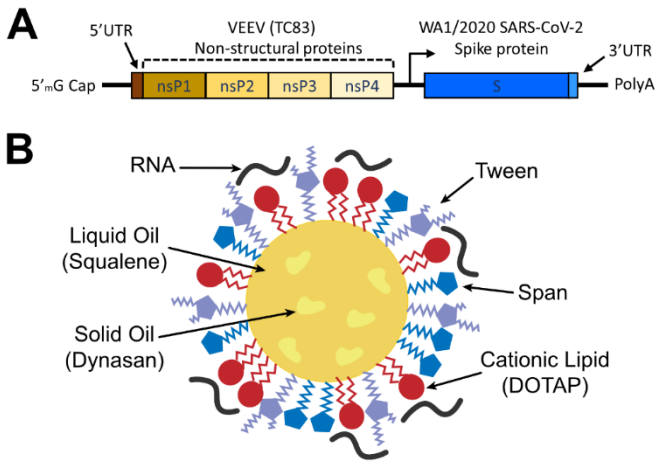

Figure 1: Design of saRNA-NLC SARS-CoV-2 vaccine AAHI-SC2. **A.** saRNA SARS-CoV-2 construct diagram. **B.** NLC diagram, complexed with RNA.

Systemic immunogenicity stimulated by i.n. saRNA-NLC vaccine

To investigate the ability of the i.n. saRNA-NLC vaccine to generate effective immunogenicity, 6-8 week old C57BL/6J mice were given prime and boost vaccine doses of 1, 5, or 10 µg, 3 weeks apart. Control mice were i.n. dosed with 10 µg of a non-immunogenic saRNA-NLC expressing the reporter protein secreted alkaline phosphatase 2 (SEAP). Systemic immunogenicity was compared between groups. Serum, bone marrow, lung, and spleen tissues were harvested after vaccination and tested for humoral (serum IgG and pseudovirus neutralization titers; bone marrow antibody-secreting cells [ASCs] by enzyme-linked immunospot [ELISpot]) and cellular (systemic T cell responses by intracellular cytokine staining and flow cytometry [ICS-flow] and T cell ELISpot of splenocytes; mucosal T cell responses by ICS-flow of lungs) vaccine-induced SARS-CoV-2-directed immune responses.

The i.n. saRNA-NLC vaccine elicited high serum IgG and SARS-CoV-2 Wuhan-strain neutralization titers that would be predicted to be protective (>1000 IC_{50}) [31,32] at all i.n. doses after prime and boost (Figure 2A, B). Strikingly, at the 10-µg dose, no significant differences were observed between i.n. and i.m. vaccines post-boost, suggesting equivalent induction of serum responses – the key correlates of protection for SARS-CoV-2 [31,32] – by the i.n. vaccine. IgG1 and IgG2a serum antibody titers indicated that i.n. vaccination with the saRNA-NLC vaccine maintains the desired Th1 bias seen with our i.m. vaccine (Figure 2C). Next, bone marrow-resident ASCs were assessed post-boost by ELISpot to determine if there was establishment of a memory niche for IgG-secreting B cells. No differences were seen between the i.n. and i.m. vaccines at either the 5- or 10-µg dose i.n. as compared to the 10-µg dose i.m. (Figure 2D), further suggesting effective systemic induction by both delivery routes and suggesting durability of response established by both vaccines.

Cell-mediated immunity, particularly T cell immunity, is also thought to be critical to sustained, long-term protection against SARS-CoV-2 [26,32]. We therefore investigated systemic cellular responses in i.n. and i.m. vaccinated mouse spleens after boost, both by ELISpot and ICS. High levels of IFNγ-secreting T cells were observed in both the i.n. and i.m. dosed mouse groups as measured by ELISpot (10-µg dose) (Figure 2E), indicating high levels of effector T cells primed to respond to SARS-CoV-2. While the levels were significantly higher in the i.m. dosed group, both groups showed robust T cell responses. IL-5- and IL-17-secreting cell levels were seen at negligible levels in either group (Figure 2F-G), suggesting a strong Th1-biased response [33,34] induced by both the i.n. and i.m. vaccines with very little induction of a potentially harmful Th2 response associated with immunopathology and natural infection [33,35,36].

These robust, strongly Th1-skewed systemic $CD4^+$ and $CD8^+$ T cell responses were verified by the use of ICS-flow performed on mouse splenocytes collected post-vaccination. After prime-boost immunization, high levels of polyfunctional ($IFN\gamma^+$, $IL\text{-}2^+$, and $TNF\alpha^+$) $CD8^+$ and $CD4^+$ T cells were observed at the 5- and 10-µg i.n. vaccine doses (Figure 2H, I), demonstrating strong T cell-mediated responses. These polyfunctional T cell levels for $CD4^+$ T cells induced by the i.n. vaccine were lower than those induced by the i.m. vaccine (20-30% reduction between the i.n. and i.m. vaccines at a 10-µg dose, $p = 0.0096$). However, $CD8^+$ T cell levels were not significantly different, and $CD4^+$ T cell responses were still high, demonstrating effective seeding of systemic T cell immunity across all i.n. and i.m. vaccinated mice. As seen with vaccine-induced antibody titers, a stronger induction of a Th1-specific response (secretion of $IFN\gamma^+$, $IL\text{-}2^+$, or $TNF\alpha^+$) compared to a Th2 response (secretion of $IL\text{-}5^+$ or $IL\text{-}10^+$) or a Th17 response (secretion of $IL\text{-}17^+$) occurred within the T cell compartment in both i.n. and i.m. vaccinated mice and across all doses (Supplementary Figure 1A), suggesting an overall systemic functional response to the virus. Overall, these data indicate that the i.n. saRNA-NLC vaccine elicits humoral and cellular responses at levels predicted to be protective.

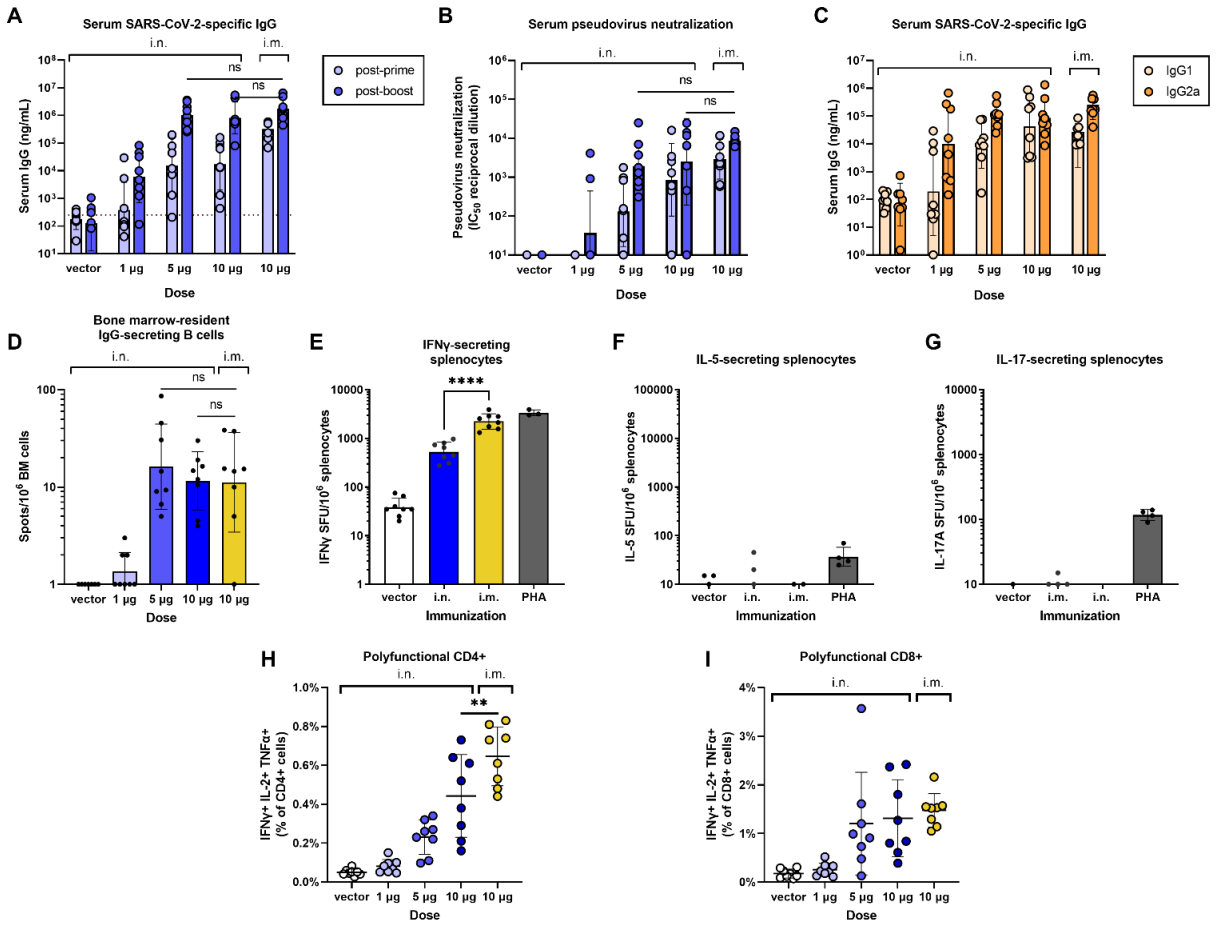

Figure 2: Systemic immunogenicity of intranasally administered SARS-CoV-2 saRNA-NLC vaccine. Systemic immunogenicity was assessed 3 weeks post-prime or post-boost in C57BL/6J mice immunized with AAHI-SC2 i.m. at 10 µg or i.n. at 1, 5, or 10 µg or with a vector control (SEAP) i.n. at 10 µg. **A.** Serum SARS-CoV-2 spike-specific IgG responses measured post-prime and post-boost. Data were log transformed and analyzed by two-way ANOVA with multiple comparisons. **B.** Serum SARS-CoV-2 Wuhan pseudovirus neutralizing titers measured post-prime and post-boost. Data were log transformed and analyzed by two-way ANOVA with multiple comparisons. **C.** Serum spike-specific IgG1 and IgG2a responses measured post-boost. **D.** Induction of bone marrow-resident spike-specific IgG-secreting B cells post-boost as measured by ELISpot. **E-G.** SARS-CoV-2 spike-responsive secretion of IFNγ, IL-5, or IL-17a by splenocytes post-boost as measured by ELISpot in mice dosed with 10 µg of saRNA. All bars

on graphs show geometric mean ± geometric SD. **H-I.** Spleen-resident spike-responsive polyfunctional T cells (IFNγ$^+$, IL-2$^+$, and TNFα$^+$ CD4$^+$ or CD8$^+$ T cells) post-boost as measured by intracellular cytokine staining and flow cytometry. Horizontal lines show mean ± SD. **p < 0.01 and ****p < 0.0001.

i.n. vaccine administration induces specialized lung T cells

While the induction of systemic responses by the i.n. vaccine, comparable to those of the i.m. vaccine, is clearly important, our main objective was to determine whether effective mucosal responses could be generated with i.n. administration of an RNA vaccine. To that end, the lung T cell compartment was analyzed from C57BL/6J mice vaccinated i.n. or i.m. with 10 µg of AAHI-SC2 3 weeks post-prime and 3 weeks post-boost; the lung T cell compartment was analyzed by ICS-flow for the presence of specialized T cell subsets that would indicate the development of long-lasting respiratory-specific immunity.

First, we examined post-vaccination lung infiltration of experienced memory T cells. These T_{RM} cells are characterized by CD69 expression as well as CD103 expression in the CD8 compartment [37]. The levels of lung-resident CD69$^+$ CD4$^+$ T cells were not significantly different between i.n. and i.m. administration (Figure 3A). However, the levels of T_{RM} cells were significantly increased in the CD8 compartment with i.n. vaccination (median of CD69$^+$ cells >20% of CD8) compared to i.m. vaccination (median of CD69$^+$ cells <10% of CD8) following boost (CD69$^+$ CD8$^+$ cells, p =0.0029; CD69$^+$ CD103$^+$ CD8$^+$, p < 0.0001) (Figure 3B, C). While the levels of these were equivalent post-prime, lung expansion of T_{RM} cells followed boost administration in the i.n. dosed group only, suggesting seeding of these durable populations followed by recall and expansion upon boost dosing.

We then assessed two other specialized T cell subsets in the lungs: CD154$^+$ T cells and CD194$^+$ T cells. CD154 (CD40 ligand [CD40L]) is often expressed on activated T cells and T follicular helper cells [38], whereas CD194 is expressed on lung-homing DC-activated T cells [39]. Here, we found similar patterns to those seen with T_{RM} cells; significantly increased populations of both CD154$^+$ CD4$^+$ and CD154$^+$ CD8$^+$ cells were observed in the lungs after i.n. saRNA vaccination post-boost compared to i.m. vaccination (p = 0.0029 and p = 0.0036, respectively) (Figure 3D, E). Likewise, a significantly higher population of CD194$^+$/CCR4$^+$ cells occurred after i.n. administration compared to i.m. administration for CD8$^+$ T cells (p = 0.0021) though not for CD4$^+$ T cells (Figure 3F-G). Collectively, these data show that i.n. administration can elicit a unique population of T_{RM}, activated, and lung-homing T cells that are within the lung and primed to respond and differentiate upon reactivation. In contrast, i.m. vaccination elicits minimal levels of these cell subsets, demonstrating that these specialized respiratory cells are not inducible by i.m. vaccination.

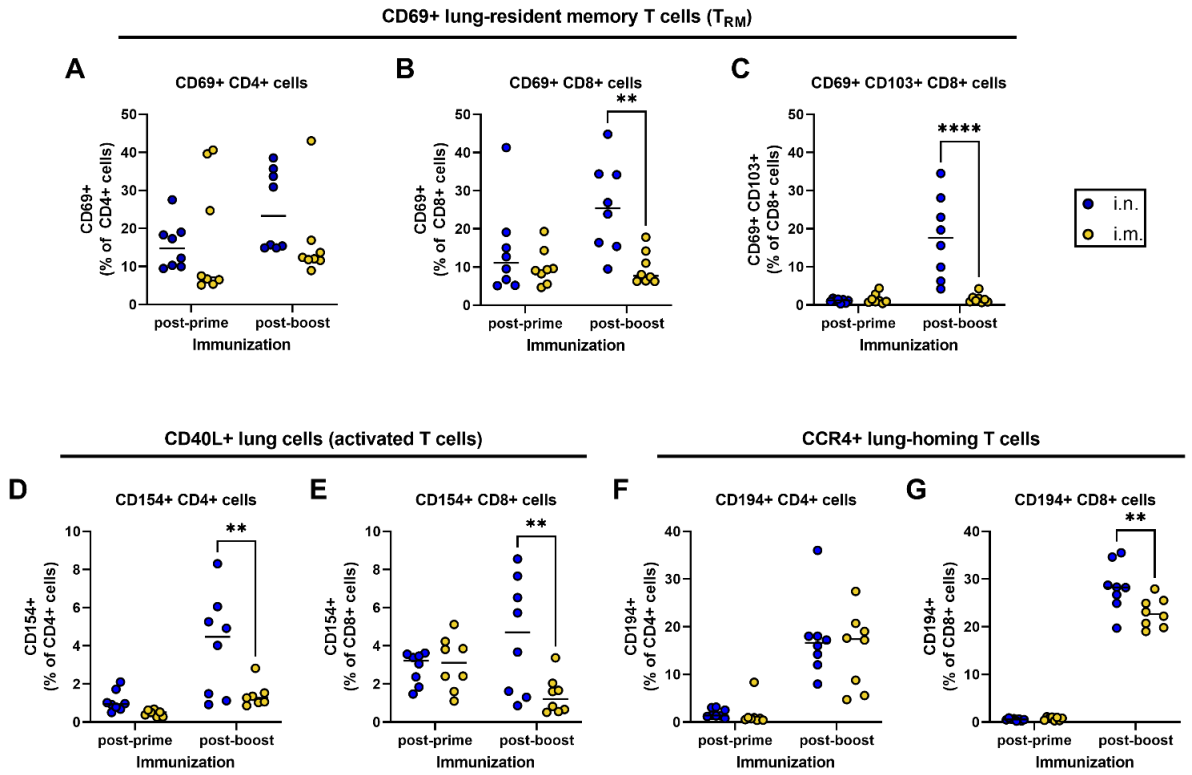

Figure 3: Mucosal T cell populations following intranasal vaccination with SARS-CoV-2 saRNA-NLC candidate. T cell populations in the lungs were assessed 3 weeks post-prime and post-boost in C57BL/6J mice immunized with 10 µg of AAHI-SC2 either i.m. or i.n after stimulation with spike peptides. **A-C**. $CD69^+$ lung-resident memory (A) $CD4^+$, (B) $CD8^+$, and (C) $CD103^+$ $CD8^+$ T cells. **D-E.** $CD40L^+$ ($CD154^+$)-expressing (D) $CD4^+$ and (E) $CD8^+$ T cells. **F-G.** $CCR4^+$ ($CD194^+$) (F) $CD4^+$ and (G) $CD8^+$ T cells. Percentage of spike-responsive cells in total live lung cells per mouse indicated by dots with horizontal line at median. $^{**}p < 0.01$ and $^{****}p < 0.0001$.

i.n. administration elicits polyfunctional respiratory response

While the lung T cell subsets were present in large populations post-i.n. administration, we wanted to verify that these cell subsets were functional as effector cells and confirm that they responded to SARS-CoV-2. Here, we took prime-boost immunized mice that had been immunized i.n. at three different doses, or i.m., with AAHI-SC2, as well as mice that received the vector control, and analyzed their CD4 and CD8 T cell polyfunctionality ($IFN\gamma^+$, $IL\text{-}2^+$, and $TNF\alpha^+$) by ICS-flow.

We first assessed the overall functionality of lung T cells and found that mice dosed i.n. with 5 or 10 µg of vaccine exhibited more polyfunctional lung T cells than the i.m. dosed mice (Figure 4A, B). Intranasally dosed mice showed a greater heterogeneity in responses than i.m. dosed mice, which we believe may be due to limitations in consistent intranasal dosing techniques for rodents. However, the peak immunogenicity was seen at the 5-µg, not the 10-µg, dose perhaps due to some low amounts of toxicity with i.n. immunization that transiently reduced mouse weights by ~10% at the 10-µg dose of vaccine (Supplementary Figure 2). This may be due to

increased quantities of NLC at the higher vaccine doses. Regardless, the 5-μg i.n. group showed significantly higher levels of polyfunctional $CD8^+$ cells ($p = 0.0157$) and a strong trend towards higher $CD4^+$ cells than the 10-μg i.m. group.

Polyfunctional IFNγ, TNFα, and IL-2-secreting SARS-CoV-2 spike-responsive T cells composed a large fraction of the key T_{RM}, $CD69^+$ population in the 5- and 10-μg i.n. immunized mice (6.70% and 2.87% of $CD4^+$ T cells and 12.8% and 9.11% of $CD8^+$ T cells, respectively), which was particularly significant in the $CD69^+$ $CD8^+$ subset of these T_{RM} cells compared to the i.m. immunized mice ($p = 0.0005$ for the 5-μg dose and $p = 0.0258$ for the 10-μg dose) as well as the $CD69^+$ $CD103^+$ $CD8^+$ subset ($p = 0.0203$) (Figure 4C-E). Intramuscularly immunized groups again induced consistently negligible levels of polyfunctional $CD8^+$ cells. We also examined the same specialized subsets, $CD154^+$/$CD40L^+$ and $CD194^+$/$CCR4^+$ cells. Similar to the T_{RM} cells, $CD154^+$ cells showed significantly higher percentages of polyfunctionally-responding cells at the 5-μg i.n. dose compared to the i.m. dose in $CD4^+$ cells ($p = 0.0006$) and a similar trend in $CD8^+$ cells (Figure 4F, G). Likewise, $CD194^+$ $CD4^+$ and $CD8^+$ cells were also induced by the i.n. vaccine at significantly higher levels at the 5-μg dose ($p = 0.0468$ and $p = 0.0071$, respectively) than the i.m. vaccine (Figure 4H, I). Collectively, these data demonstrate that i.n. administration is seeding specialized T cell populations in the lung that are highly polyfunctional cell subsets but are absent with i.m. administration.

Lastly, we estimated the response quality of the lung T cells to confirm that i.n. administration elicited Th1-biased lung T cell responses, similar to what was observed in the spleen. The majority of the responses to both the i.n. and i.m. vaccines were Th1-specific responses, with some Th2 responses and negligible Th17 responses (Supplementary Figure 1B), similar to what was observed in the spleen. Additionally, the Th2 response (IL-5 expression) did not scale with

increasing dosage, suggesting a baseline level of IL-5 expression in lung T cells rather than a Th2 response specifically induced by the vaccine.

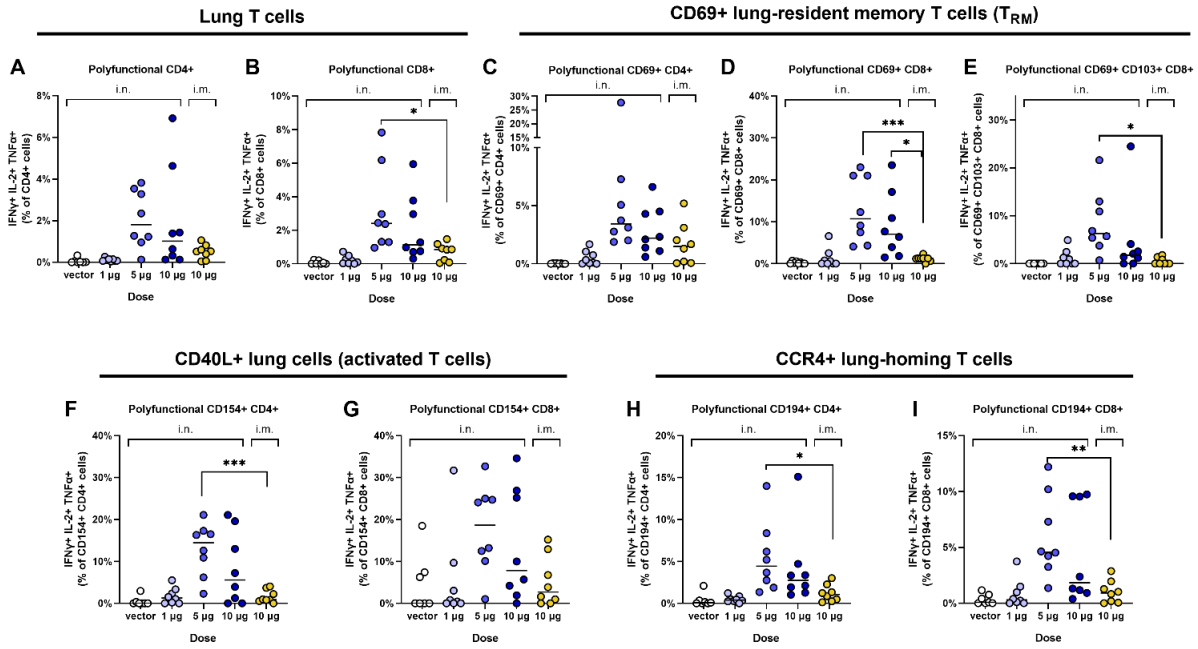

Figure 4: Mucosal SARS-CoV-2 spike polyfunctionally-reactive T cell populations following immunization with the intranasal or intramuscular SARS-CoV-2 saRNA-NLC vaccine. T cell populations in the lungs were stimulated with SARS-CoV-2 spike peptides for 6 hours and stained for T cell markers and cytokine expression 3 weeks post-prime or post-boost in C57BL/6J mice immunized with 1, 5, or 10 µg of the i.n. saRNA-NLC vaccine, relative to 10 µg of the i.m. vaccine or an i.n. vector control (SEAP) saRNA-NLC. Percentages of polyfunctional cells (expressing IFNγ, IL-2, and TNFα) were then measured by flow cytometry. **A-B.** Lung-resident (A) $CD4^+$ and (B) $CD8^+$ T cells. **C-E.** $CD69^+$ lung-resident memory (C) $CD4^+$, (D) $CD8^+$, and (E) $CD103^+$ $CD8^+$ T cells. **F-G.** CD40L-expressing ($CD154^+$) (F) $CD4^+$ and (G) $CD8^+$ T cells. **H-I.** CCR4-expressing ($CD194^+$) lung-homing (H) $CD4^+$ and (I) $CD8^+$ T cells. Dots

represent values measured from individual mice. Horizontal lines indicate data median. Significance determined by two-way ANOVA: *$p < 0.05$, **$p < 0.01$, and *** $p < 0.001$.

Heterologous dosing for systemic and mucosal responses

To next understand whether i.n. administration could be viable as a boosting strategy for individuals previously vaccinated with an i.m. SARS-CoV-2 vaccine, we examined mice that were primed with an i.m. vaccine and then boosted with a medium dose (5 µg) either i.m. or i.n. Intranasally boosted mice showed equivalent systemic neutralizing antibody responses to the i.m. boosted mice (Figure 5A, B). Within the T cell compartments, i.n. boost immunization induced equivalent or increased spleen-resident polyfunctional T cell responses in $CD4^+$ or $CD8^+$ ($p = 0.0454$) cells, respectively, compared to an i.m. boost immunization (Figure 5C, D), indicating, that an i.n. booster may effectively boost the systemic immunity developed in response to an original i.m. vaccination. Most importantly, the i.n. booster elicited significantly more polyfunctional lung-resident $CD8^+$ T_{RM} cells ($p = 0.0236$) than the i.m. booster (Figure 5E, F), indicating that just boosting with an i.n. dose may be sufficient to get the full mucosal immune-stimulating effect of i.n. vaccination. These data are consistent with other i.n. vaccines that suggest i.n. dosing can have enhanced efficacy systemically as compared to i.m. vaccines [13]. This suggests that an i.n. boost vaccination strategy may be ideal to boost systemic and induce respiratory immunity in previously vaccinated individuals, reflecting the real-world scenario of second-generation SARS-CoV-2 vaccine rollouts.

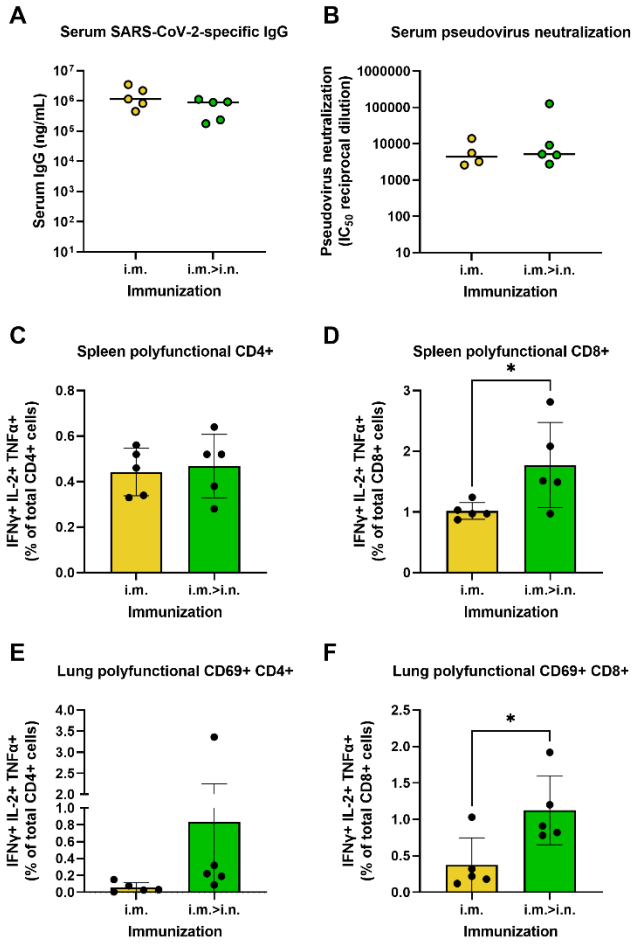

Figure 5: Systemic and mucosal immune responses following boost immunization with the intranasal or intramuscular SARS-CoV-2 saRNA-NLC vaccines. 10-week-old C57BL/6J mice were injected i.m. with a 10-µg prime dose (N:P of 15) and then boosted with a 5-µg dose of either the i.n. or i.m. saRNA-NLC vaccine 7 weeks later. **A.** SARS-CoV-2 spike-specific IgG titers as measured by ELISA 3 weeks post-boost. Horizontal lines show median. **B.** Serum SARS-CoV-2 pseudovirus neutralizing titers 3 weeks post-boost. Horizontal lines show median. **C-D.** Spleen polyfunctional T cell responses. **E-F.** Polyfunctional lung-resident memory T cell responses. Statistics evaluated as *t*-tests, *$p < 0.05$. Bars on graphs show mean with SD.

Long-term immunogenicity of vaccine dosing strategies

Finally, we assessed the ability of these i.m. and i.n. vaccination regimes to maintain immunogenicity over a more extended timeframe. To do so, we compared humoral and cellular immune responses in mice 4 months after i.m.-only prime-boost, i.n.-only prime-boost, or i.m.-prime followed by i.n.-boost vaccination regimes.

Overall, systemic humoral immunity was retained in all groups from post-boost peak responses (5 weeks post-prime) to the end of the experiment (4 months post-boost) (Figure 6A). No significant differences were observed in any vaccination regime between these two timepoints, nor between the three vaccination regimes despite a higher trend in the homologous i.m. group. Similarly, no significant differences were observed in pseudoneutralization across timepoints or vaccination regimes (Figure 6B). These data further validate the viability of all three vaccine regimens as durable vaccine immunizations, showing retention of neutralizing antibodies, the putative correlate of protection, without evidence of waning over a 4-month period. Likewise, lung and bone marrow tissues contained equivalent levels of SARS-CoV-2 spike-reactive IgG-secreting cells as measured by ELISpot across all mouse groups, with a trend towards higher IgG in the lung after the heterologous i.m.-i.n. vaccination regime (Figure 6C, D).

Next, we investigated the T cell responses in the spleen and lung, thought to be key to long-term immunity and reduction of infection severity [26], 4 months post-boost**.** While T cell responses in spleens showed expected declines from peak immunogenicity (Figure 2, Figure 4), particularly in the CD4 subset, significant levels of polyfunctional $CD4^+$ and $CD8^+$ cells were retained in all groups (Figure 6E, F). The homologous i.m. and heterologous i.m.-i.n. vaccinated groups showed the highest SARS-CoV-2 spike-responsive $CD4^+$ T cell polyfunctionality in

mouse spleens, significantly higher than those seen in the homologous i.n. vaccinated mice ($p < 0.0045$ for both). However, in the lung cells, the heterologous i.m.-i.n. vaccinated mice showed the highest induction of polyfunctional lung $CD4^+$ and $CD8^+$ cells (Figure 6G, H), and outperformed both the homologous i.n. and i.m. groups. Boosting of previous i.m. vaccination with an i.n. vaccine induced the most potent response in both the spleens and the lungs, and retained durable humoral and cellular immunity throughout 4 months after vaccination, indicating that i.n. vaccination with an saRNA-NLC vaccine may be a viable long-term strategy to bolster existing immunity.

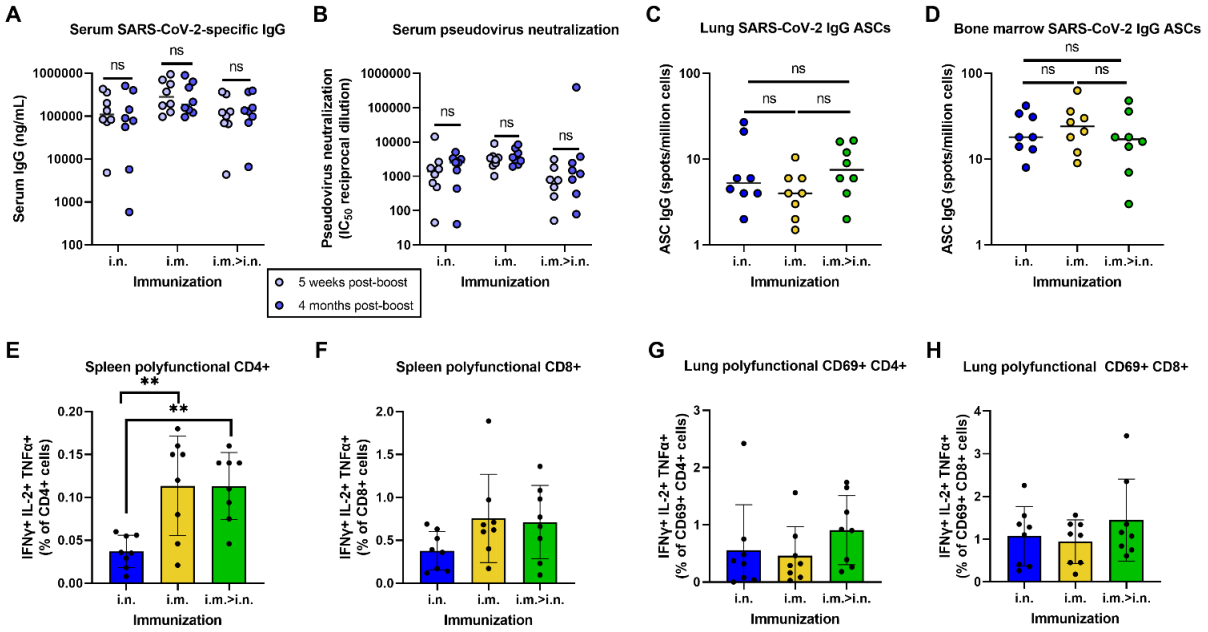

Figure 6: Long-term durability of immunity following immunization strategies with SARS-CoV-2 saRNA-NLC vaccine candidate. Serum and T cell populations were assessed in mice 4 months after homologous i.n., homologous i.m., or i.m. prime and i.n. boost vaccination regimes. Each dose was 10 µg. **A.** Serum SARS-CoV-2 spike-specific IgG titers as measured by ELISA 5 weeks and 4 months post-boost. **B.** Serum SARS-CoV-2 pseudovirus neutralizing

titers at 5 weeks and 4 months post-boost. **C-D.** ELISpot analysis of bone marrow and lung SARS-CoV-2-binding IgG-secreting cells at 4 months post-boost. **A-D.** Horizontal lines show median. **E-F.** Spleen SARS-CoV-2-reactive polyfunctional T cell responses. **G-H.** Lung-resident SARS-CoV-2-reactive polyfunctional memory T cell responses. Bar graphs show mean with SD. Statistical analysis by one-way ANOVA with Tukey's multiple comparison test. ** $p < 0.01$.

Discussion

Here we show, for the first time, delivery of an i.n. RNA vaccine that induces key respiratory mucosal immune responses. This i.n. administered saRNA vaccine was able to induce systemic immunity, in both the humoral and cellular compartments, that rivaled i.m. administration. Unlike i.m. administration, i.n. administration elicited not only high levels of polyfunctional T cells in the spleen but also in the lung, demonstrating a novel induction of key respiratory mucosal T cell populations by an RNA vaccine [40–42]. Furthermore, we were able to demonstrate potential for this product as an i.n. booster of prior i.m. vaccine-induced immunity, a common real-life scenario given the largely COVID-experienced population at this point in the pandemic. This i.n. boost of prior i.m. vaccine-induced immunity significantly boosted systemic responses in addition to inducing mucosal T cell populations not stimulated by i.m. vaccine boosting. Lastly, we showed that, when used as a booster of prior i.m. vaccine responses, the i.n. dose elicited the development of durable immunity, retaining its humoral and cellular efficacy for at least 4 months in mice.

Now in the third year of the COVID-19 pandemic, second-generation SARS-CoV-2 vaccines are urgently needed. While several vaccines have been developed and approved in the last 2.5 years, many utilizing novel mRNA vaccine technologies [43–45], which have admirably contributed

to the waning of disease mortality globally [46], emerging trends highlight the insufficiencies of current vaccine approaches. Vaccine efficacy has waned rapidly [47–50], and frequent boosters have been recommended for individuals that received the Pfizer and/or Moderna mRNA vaccines [48,49,51]. Increasing evidence of reinfection, both post-infection and post-vaccination [52], particularly with the Omicron variant [53], has negatively impacted vaccine credibility. With the ongoing pandemic predicted to remain a present threat, new variants will continually place pressure on the efficacy of these first-generation vaccines [54,55].

While more research is necessary as to why current vaccines are waning, emerging research is pointing to insufficient nasal and mucosal immunity. Increasingly, data are demonstrating that i.m. vaccination alone is insufficient to generate potent mucosal immunity that is predicted to be critical for early control and clearance of SARS-CoV-2 [56]. Vaccinees still show evidence of viral RNA in the upper respiratory tract after viral exposure, suggesting ongoing viral replication and transmission [12,14,57] even by vaccinated populations. However, breakthrough infection with SARS-CoV-2 allows vaccinees to elicit potent mucosal and nasal immunity [40–42]. Thus, improving the induction of nasal and mucosal immunity following vaccination is a critical component for second-generation vaccines to finally achieve durable and flexible protection. However, data also show that generating this immunity is not possible via standard i.m. vaccination and likely requires administration of an i.n. vaccine [58].

AAHI's i.n. SARS-CoV-2 saRNA-NLC vaccine candidate elicits not only systemic humoral immunity but also high levels of polyfunctional T cells, both systemically and within the lungs, suggesting broad T cell presence across the respiratory tract – an effect that i.m. delivered mRNA vaccines are unable to induce [40–42]. While CD4 and CD8 T cell levels are now being recognized as a major determinant of disease progression and critical to long-lasting immunity

[26], the main vaccines on the market elicit minimal peripheral T cell responses [59,60] and negligible mucosal/respiratory T cell responses [40–42]. In contrast, AAHI's i.n. saRNA-NLC vaccine candidate elicits and retains high levels of polyfunctional T cells for at least 4 months post-boost. These T cell populations, along with the lack of waning humoral responses in this timeframe, suggest that this i.n. saRNA vaccine candidate may induce substantially more durable protective immune responses than existing mRNA vaccines. Finally, these data demonstrate the potential for this i.n. saRNA-NLC vaccine candidate as an i.n. booster to pre-existing SARS-CoV-2 immunity, outperforming an i.m. booster, showing that the additive effect of this i.n. vaccine to pre-existing systemic immune responses generated the greatest benefit of all vaccination regimens tested.

Intranasal vaccines to date have primarily been developed as live-attenuated flu vaccines, including FluMist [61]. Recently, four new i.n. or inhalable vaccines have been approved for SARS-CoV-2 in China, India, Iran, and Russia, including two adenovirus-vectored vaccines [62–64]. Further development of nasal or airway administration of vaccines for influenza and other respiratory viruses has remained an attractive target given the potential for development of critical airway T_{RM} cells at this first line of defense [3,65]. Several other i.n. vaccines are in development for SARS-CoV-2, but most rely on standard protein or adenovirus vector vaccine technologies [12,13,42,66,67]. Validating an RNA-based, i.n. administered vaccine technology would be a significant development not only for the SARS-CoV-2 pandemic but for other respiratory pathogens, combining the rapidity and reliability of RNA vaccine adaptation to new targets with the key mucosal immune responses induced by mucosal-specific dosing.

While the homologous i.n. prime-boost saRNA-NLC vaccine induces excellent systemic and mucosal immune responses, the i.n. saRNA vaccine may be most effective as a booster dose

for previously i.m. vaccinated individuals. This result aligns with the results of other studies [27,57,68] where priming an immune response with a strong i.m. vaccine followed by i.n. vaccination is able to optimally stimulate the T_{RM} compartment while still boosting the extant i.m. induced immunity. Our data demonstrate the clear potential of using an identical or similar RNA vaccine product for both i.m and i.n. vaccination, potentially eliminating many manufacturing hurdles and using an already clinically tested vaccine platform technology [69]. Particularly, i.n. boosting outperformed i.m. boosting, hinting at the potential for i.n. dosing to access novel cell compartments and mechanisms. Further work remains to fully optimize the i.n. saRNA vaccine formulation specifically for i.n. administration, potentially including use of nasal spray devices, with the goal of enhancing induction of immunity while avoiding toxicity – toxicity signals are currently only seen transiently at high (≥10 ug) doses in mice suggesting a broad safe range for dosing in larger animals – as well as reducing the heterogeneity in responses. This i.n. vaccine candidate is currently in large primate studies on track to enable toxicity studies and future human testing.

This i.n. saRNA-NLC vaccine technology represents a promising vaccine platform to combat both the existing SARS-CoV-2 pandemic and other respiratory illnesses, such as seasonal and pandemic influenza. For respiratory pathogens, i.n. vaccination or i.n. vaccine boosting of i.m. vaccination may help raise RNA vaccine technologies to a new level, through stimulating respiratory T cell populations [70,71] and generating effector subsets within the lungs and nasal mucosa primed to respond rapidly at the first point of infection [57]. Beyond its efficacy at stimulating T_{RM} subsets and bolstering systemic immunity, i.n. administration may also be desirable as a needle-less delivery method with potentially higher uptake, particularly in pediatric and vaccine-hesitant populations. Altogether, this novel demonstration of a unique i.n.

delivered RNA vaccine that elicits strong systemic and mucosal immunity is an indication of a promising new technology ripe for future development and application.

Methods

saRNA expression plasmid design, cloning, and production

The saRNA plasmid was designed and selected based on immunogenicity measures from i.m. immunization [24]. Briefly, the saRNA encodes a SARS-CoV-2 spike sequence based on a GenBank sequence (MT246667.1) containing the D614G mutation, a diproline at sites 987-988, and a QQAQ substitution for RRAR in the furin cleavage site (683-686). The sequence was codon-optimized for expression in humans, synthesized by BioXp, and inserted via Gibson cloning into AAHI's backbone saRNA expression vector. A SEAP-expressing plasmid was also used as a control, created similarly with the SEAP sequence in the place of the vaccine antigen. Sanger sequencing was used to confirm plasmid sequences. These were then amplified in *Escherichia coli* and extracted using Qiagen maxi- or gigaprep kits, linearized with NotI (New England Biolabs), and purified using a Qiagen DNA purification kit.

RNA manufacture

NotI-linearized DNA plasmids containing T7 promoters were used as templates for *in vitro* transcription (IVT) of saRNA for vaccination. Our in-house optimized IVT protocol with T7 polymerase, RNase inhibitor, and pyrophosphatase (Aldevron) was used. Next, a DNase step was used to digest the templates, and Cap0 structures were added to the RNA transcripts with guanylyltransferase (Aldevron), GTP, and S-adenosylmethionine (New England Biolabs). CaptoCore 700 resin (GE Healthcare) was used to chromatographically purify the RNA followed by diafiltration and concentration. saRNA material was filtered through a 0.22-µm polyethersulfone filter and stored at −80°C until further use. saRNA size and integrity was

characterized by gel electrophoresis, and RNA concentration was quantified by UV absorbance (NanoDrop 1000) and RiboGreen assay (Thermo Fisher).

NLC manufacture

A mixture of trimyristin (IOI Oleochemical), squalene (Sigma-Aldrich), sorbitan monostearate (Sigma-Aldrich), and the cationic lipid 1,2-dioleoyl-3-trimethylammonium-propane (DOTAP; Corden) was heated at 70°C in a bath sonicator. Separately, polysorbate 80 (Fisher Scientific) was diluted in 10 mM sodium citrate trihydrate and heated to 70°C in a bath sonicator. After all components were in suspension, a high-speed laboratory emulsifier (Silverson Machines) running at 7,000 rpm was used to blend the oil and aqueous phases. Particle size of the mixture was further decreased through high-shear homogenization. The colloid mixture was then processed at 30,000 psi for 11 discrete microfluidization passes using an M-110P microfluidizer (Microfluidics). The NLC product was then filtered through a 0.22-µm polyethersulfone filter and stored at 2°C–8°C until use [24,30,72].

Vaccine complexing and characterization

Vaccine complexes for immediate inoculation into mice were produced by combining aqueous RNA at a 1:1 volume ratio with NLC that was pre-diluted in a 10 mM sodium citrate and 20% w/v sucrose buffer. Vaccines were prepared at a nitrogen:phosphate (N:P) ratio of 5-15, representing the ratio of amine groups on the NLC DOTAP to the RNA's backbone phosphate groups. This complexing resulted in vaccine containing the intended dose of complexed saRNA-NLC in an isotonic 10% w/v sucrose, 5 mM sodium citrate solution. The vaccine solution was incubated on ice for 30 minutes after mixing to ensure complete complexing.

Mouse studies

All animal work was done according to the Bloodworks Northwest Research Institute's Institutional Animal Care and Use Committee. All animal work was in compliance with all applicable sections of the Final Rules of the Animal Welfare Act regulations (9 CFR Parts 1, 2, and 3) and the *Guide for the Care and Use of Laboratory Animals* [73].

C57BL/6J mice purchased from The Jackson Laboratory were used for all animal studies. Mice were between 6 and 8 weeks of age at study onset. At arrival, mice were simultaneously randomized into study groups. Mouse technicians were not blinded to study groups. After 1 week of acclimatization to the facility, mice were then primed with vaccine. Mice were then boosted 3 weeks later and harvested 3 weeks after boost. Mouse weights were monitored for 4 days following prime and boost vaccination. Mice were immunized by i.m. injection in both rear quadriceps muscles (50 µL/leg, 100 µL total) or by i.n. inoculation in two 25 µL doses. Intranasal inoculation was done under full anesthesia, and mice were allowed to recover under a heat lamp. During ongoing studies, serum samples were taken by retro-orbital bleed. Three-weeks post-boost, mice were harvested, terminal bleeds were taken, spleens and lungs were dissected, and femurs were harvested for bone marrow purification.

Serum IgG, IgG1, and IgG2a titers by ELISA

SARS-CoV-2 spike-specific IgG was measured by enzyme-linked immunosorbent assay (ELISA). Plates (Corning 384-well high-binding #CLS3700) were coated with Recombinant SARS-Cov-2 Spike His Protein, Carrier Free (R&D Systems #10549-CV), at 1 µg/mL and incubated overnight at 4°C. Plates were incubated in blocking buffer (2% dry milk, 0.05% Tween 20, 1% goat serum) for over 1 hour. Samples were plated on low-binding plates, starting at a dilution of 1:40 and then serially diluting 1:2 across the plate. High-binding plates were washed, and samples were then transferred from the low-binding plates to the coated, high-binding

plates. Naive mice serum at 1:40 was used as a negative control. A SARS-Cov-2 neutralizing monoclonal antibody (GenScript #A02057) was used as a positive control at a starting concentration of 3.2 ng/µL. Following a 1-hour incubation, plates were washed, and a secondary antibody, Anti-Mouse IgG (Fc Specific)-Alkaline Phosphatase antibody (Sigma-Aldrich #A2429), at a 1:4000 dilution was added. Following the secondary antibody and another wash step, phosphatase substrate tablets (Sigma-Aldrich #S0942) were dissolved in diethanolamine substrate buffer (Fisher Scientific #PI34064) at a final concentration of 1 mg/mL and added to the plates. Plates were incubated for 30 minutes and then read spectrophotometrically at 405 nm. A 4-point logistic (4PL) curve was used to fit the antibody standard titration curve, and sample concentrations were interpolated off the linear region of the curve.

For IgG1 and IgG2a isotype-specific ELISAs, plates were coated and blocked as described above. For IgG1 and IgG2a, the standard curve was run using SARS-CoV-2 neutralizing antibodies (GenScript #A02055 and #BS-M0220, respectively). Sample dilution and incubation were identical to the total IgG curve, and plates were probed with IgG1- and IgG2a-specific secondary alkaline phosphatase (AP)-conjugated detection antibodies (Sigma-Aldrich #SAB3701172 and #SAB3701179, respectively) prior to development, reading, and quantification as described above.

Pseudovirus neutralization assay

SARS-CoV-2 pseudovirus neutralizing antibody titers in mouse sera were measured via a pseudoneutralization assay [74]. Lentiviral SARS-CoV-2 spike protein pseudotyped particles were prepared by co-transfecting HEK-293 cells (American Type Culture Collection CRL #11268) with plasmids containing a lentiviral backbone-expressing luciferase and ZsGreen (BEI Resources #NR-52516), lentiviral helper genes (BEI Resources

#NR-52517, NR-52518, and NR-52519), or a delta19 cytoplasmic tail-truncated SARS-CoV-2 spike protein (Wuhan strain plasmids from Jesse Bloom of Fred Hutchinson Cancer Center). Cells were incubated for 72 hours at standard cell culture conditions (37°C, 5% CO_2), and cell culture media was harvested and filtered through a 0.2-µm filter. Pseudovirus-containing supernatant was frozen until titering and use.

To perform the assay, plates were seeded with Human Angiotensin-Converting Enzyme 2 (hACE2)-expressing HEK-293 cells (BEI Resources #NR52511) and incubated overnight. Serum samples were pre-diluted 1:10 in media (Gibco Dulbecco's Modified Eagle Medium + GlutaMAX + 10% fetal bovine serum [FBS]) and then serially diluted 1:2 for 11 total dilutions. These were then incubated with polybrene (Sigma-Aldrich #TR-1003-G) and pseudovirus for 1 hour. Then, the serum samples were added onto the hACE2 cells in duplicate and incubated at 37°C and 5% CO_2 for 72 hours. To determine 50% inhibitory concentration (IC_{50}) values, plates were scanned on a fluorescent imager (Molecular Devices ImageXpress Pico Automated Cell Imaging System) for ZsGreen expression. Total integrated intensity per well was used to calculate the percent of pseudovirus inhibition per well. Neutralization data for each sample were fit with a 4-parameter sigmoidal curve, which was used to interpolate IC_{50} values.

Spleen, lung, and bone marrow cell harvest

Spleens were prepared in 4 mL of RPMI medium by manual maceration through a filter using the back of a syringe. Dissociated splenocyte samples were centrifuged briefly at 400 x g to pellet fat cells, and the supernatants containing lymphocytes were either transferred to 5-mL mesh-cap tubes to strain out any remining tissue debris or lysed with ammonium-chloride-potassium (ACK) lysing buffer. Cells were counted on a Guava easyCyte cytometer (Luminex) and plated in round-bottom 96-well plates at 1-2 x 10^6 cells per well in complete RPMI (cRPMI) medium containing CD28 costimulatory antibody (BD Biosciences #553294) and brefeldin A.

One of three stimulation treatments was added to each well: 0.0475% dimethyl sulphoxide [DMSO], 2 µg/µL spike peptide pool (JPT peptides #PM-WCPV-S-1), or phorbol myristate acetate (PMA)-ionomycin. Plates were incubated for 6 hours at 37 C with 5% CO_2.

Lung cells were isolated via enzymatic digestion using a gentleMACS Dissociator (Miltenyi Biotec). Lungs were dissociated in 4 mL of Hanks' Balanced Salt Solution (HBSS) supplemented with 10% Liberase (MilliporeSigma), 10% aminoguanidine, 0.1% KN-62, and 1.25% DNase. Lungs and enzymatic mix were added to a gentleMACS M tube (Miltneyi Biotec), and the m_lung_01.02 program was run. Samples were then incubated at 37°C and 5% CO_2 for 30 minutes. Directly after, samples were run again on the gentleMACS Dissociator using the m_lung_02.01 program. The resulting slurry was added to 10 mL of RPMI medium and centrifuged for 5 minutes. The supernatant was discarded, and the cells were either filtered through a 5-mL snap-top tube or washed again in RPMI medium prior to counting on a Guava easyCyte cytometer and plated in round-bottom 96-well plates at 1-2 x 10^6 cells per well in RPMI medium containing 10% FBS, 50 µM beta-mercaptoethanol, CD28 costimulatory antibody, brefeldin A, and one of three stimulation treatments: 0.0475% DMSO, 2 µg/µL spike peptide pool (JPT peptides #PM-WCPV-S-1), or PMA-ionomycin. Plates were incubated for 6 hours at 37 C with 5% CO_2.

Intracellular cytokine staining and flow cytometry

Following incubation, plates were centrifuged at 400 x g for 3 minutes, the supernatants were removed, and cells were resuspended in phosphate-buffered saline (PBS). Splenocytes were stained for viability with Zombie Green (Biolegend) in 50 µL of PBS. Cells were washed twice, and then spleen samples were incubated with CD16/CD32 antibody (Invitrogen #14-0161-86) to block Fc receptors. Next, the cells were surface stained in an additional 50 µL of staining buffer (PBS with 0.5% bovine serum albumin and 0.1% sodium azide). Spleen samples were stained

with fluorochrome-labeled monoclonal antibody (mAb) specific for mouse CD4 (eBioscience #45-0042-82), CD8 (BD Biosciences #563068), CD44 (BD Biosciences #560568), and CD107a (BioLegend #121614), while lung samples were stained for CD4 (BioLegend #100526), CD8 (BD Biosciences #563068), CD44 (BD Biosciences #562464), CD69 (BioLegend #104508), CD103 (BioLegend #121435), CD194 (BioLegend #131220), and CD154 (BD Biosciences #745242). Cells were washed twice, permeabilized using the Fixation/Permeabilization Kit (BD Biosciences #554714), and stained intracellularly. Spleens were stained for TNFα (BioLegend #506327), IL-2 (BioLegend #503824), IFNγ (Invitrogen #25731182), IL-5 (eBioscience #12-7052-82), IL-10 (BD Biosciences #564081), and IL-17a (BD Biosciences #560820), while lungs where stained for TNFα (BioLegend #506327), IL-2 (BioLegend #503824), IFNγ (Invitrogen #25731182), IL-5 (BioLegend #504306), and IL-17a (BD Biosciences #560820). After two washes in staining buffer, cells were resuspended in 100 µL of staining buffer and analyzed using an LSRFortessa flow cytometer (BD Biosciences). After initial gating for live $CD4^+$ or $CD8^+$ lymphocytes, cells gating positive for all three activation markers IL-2, IFNγ, and TNFα were counted as activated polyfunctional T cells.

Bone marrow harvest and B cell ELISpot

Antibody-secreting bone marrow-resident cell levels were measured by ELISpot. $MultiScreen_{HTS}$ IP Filter plates (0.45 µm, MilliporeSigma) were treated with 15 µL of 35% ethanol for 30 seconds. Recombinant SARS-CoV-2 Spike His Protein, Carrier Free (R&D Systems #10549-CV-100), was diluted at 2 µg/mL in ELISpot coating buffer (eBioscience), and plates were coated with 100 µL. Plates were incubated overnight at 4°C. The next day, plates were washed with PBS with 0.1% Tween 20 and blocked with cRPMI medium for 2 hours.

Femurs were removed from mice and inserted into a snipped-end 0.6-mL Eppendorf tube and then inserted into a 1.5-mL Eppendorf tube with 1 mL of cRPMI medium. Femurs were centrifuged for 15 seconds at 10,000 rpm, and supernatant was discarded. Cell pellets were vortexed, resuspended in 200 µL of RBC Lysis Buffer (Invitrogen), and then incubated on ice for 30 seconds. An additional 800 µL of RPMI medium was added, and cells were centrifuged for 5 minutes at 400 x g before the supernatant was decanted. Cells were resuspended in 1 mL of cRPMI medium, counted, and transferred to prepared filter plates at 1 million cells per well followed by a 3-fold dilution across five adjacent wells.

Plates were incubated for 3 hours, then washed three times with PBS plus 0.1% Tween 20. Secondary antibody (Goat Anti-Mouse IgG-HRP or IgA-HRP [SouthernBiotech #1030-05 and #1040-05, respectively]) was added at a 1:1000 dilution in PBS with 0.1% Tween and 5% FBS overnight at 4°C. Plates were then washed three times in PBS with 0.1% Tween 20 and two times in PBS. 100 µL of Vector NovaRED Substrate Peroxidase (Vector Laboratories #SK-4800) was applied for 7 minutes to develop the plates. The reaction was quenched by rinsing plates with distilled water for 2 minutes, and plates were dried in the dark. Spots were counted and data were analyzed using ImmunoSpot v7 software (Cellular Technology Limited).

T cell ELISpot assay

IFNγ (BD Biosciences #51-2525KZ), IL-17A (Invitrogen #88-7371-88), or IL-5 (BD Biosciences #51-1805KZ) at a 1:200 dilution in Dulbecco's PBS (DPBS; Gibco) was used to coat ELISpot plates (MilliporeSigma). Plates were incubated overnight at 4°C and then washed and blocked with cRPMI medium for at least 2 hours. Previously harvested splenocytes (see above) were added at 2 x 10^5 cells per well. Samples were then stimulated with 1 µg/mL PepMix SARS-CoV-2 (JPT Peptide Technologies #PM-WCPV-S-1). Plates were incubated at 37°C and 5% CO_2 for

48 hours. Then plates were washed with PBS with 0.1% Tween 20. Next, detection antibody (IFNγ, BD Biosciences #51-1818KA; IL-17A, Invitrogen #88-7371-88; and IL-5, BD Biosciences #51-1806KZ) was diluted in ELISpot diluent (eBiosciences) at 1:250 and added overnight at 4°C. Plates were washed and then developed using Vector NovaRED Substrate Peroxidase for 15 minutes. The reaction was quenched with deionized water. Plates were then dried in the dark. Spots were counted and data were analyzed using ImmunoSpot.

Statistical analysis

CD4 and CD8 cell polyfunctionality was assessed by one-way ANOVA with Tukey's multiple comparison test. The effect of timepoint on IgG titer and pseudoneutralization was assessed in log-transformed data with a two-way ANOVA with Tukey's multiple comparison test or using a mixed-effects model with Sidak's multiple comparison test if some sample data were missing. Lung or bone marrow ELISpot IgG was analyzed using log-transformed data with one-way ANOVA with Tukey's multiple comparison test.

Acknowledgments

We thank Jesse Bloom (Fred Hutchinson Cancer Center) for sharing the SARS-CoV-2 spike protein plasmids used in pseudovirus production. We are additionally grateful to Robert Kinsey, who conducted the manufacture of the NLC used in these studies; Christopher Press, who manufactured some RNA products used in this study; Jeff Guderian; and Ethan Lo. We also thank Theresa Britschgi, who was instrumental as project manager for this work, and Valerie Soza, for editorial assistance. This work was funded in part by sponsored research from ImmunityBio, Inc. The content is solely the responsibility of the authors and does not necessarily represent the views of the funders.

Author Contributions

M.F.J and E.A.V conceived the studies. M.F.J, E.A.V., and A.G. supervised the research and administered the project. E.A.V. and C.C. acquired funding. M.F.J., S.B., D.H., P.B., J.B., D.H., R. M., J.S., N.C., and S.R. contributed to the investigation. M.F.J. curated the data. M.F.J., S.B., P.B., N.C., and E.A.V. analyzed the data. M.F.J and E.A.V. wrote the first draft of the manuscript. All authors reviewed and edited the manuscript.

Competing Interests

A.G. and E.A.V. declare no Competing Non-Financial Interests but the following Competing Financial Interests. A.G. and E.A.V. are co-inventors on PCT patent application PCT/US21/40388, “Co-lyophilized RNA and Nanostructured Lipid Carrier,” and related national filings, as well as U.S provisional patent application 63/345,345, “Intranasal Administration of Thermostable RNA Vaccines,” and 63/144,169, “A thermostable, flexible RNA vaccine delivery platform for pandemic response.” All other authors declare they have no competing interests.

Data Availability

The datasets generated during and/or analysed during the current study are available from the corresponding author on reasonable request.

Materials & Correspondence

Correspondence and material requests should be addressed to the corresponding author Emily A. Voigt at emily.voigt@aahi.org.

References

1. Mouro, V. & Fischer, A. Dealing with a mucosal viral pandemic: lessons from COVID-19 vaccines. *Mucosal Immunol* 1–11 (2022) doi:10.1038/s41385-022-00517-8.

2. Kissler, S. M. *et al.* Viral dynamics of SARS-CoV-2 variants in vaccinated and unvaccinated persons. *New England Journal of Medicine* (2021) doi:10.1056/NEJMc2102507.
3. Tiboni, M., Casettari, L. & Illum, L. Nasal vaccination against SARS-CoV-2: synergistic or alternative to intramuscular vaccines? *Int J Pharm* **603**, 120686 (2021).
4. Garcia-Knight, M. *et al.* Infectious viral shedding of SARS-CoV-2 Delta following vaccination: A longitudinal cohort study. *PLOS Pathogens* **18**, e1010802 (2022).
5. Chen, J., Wang, R., Gilby, N. B. & Wei, G.-W. Omicron variant (B.1.1.529): infectivity, vaccine breakthrough, and antibody resistance. *J. Chem. Inf. Model.* **62**, 412–422 (2022).
6. Feikin, D. R. *et al.* Duration of effectiveness of vaccines against SARS-CoV-2 infection and COVID-19 disease: results of a systematic review and meta-regression. *The Lancet* **399**, 924–944 (2022).
7. Link-Gelles, R. *et al.* Effectiveness of 2, 3, and 4 COVID-19 mRNA vaccine doses among immunocompetent adults during periods when SARS-CoV-2 Omicron BA.1 and BA.2/BA.2.12.1 sublineages predominated — VISION network, 10 states, December 2021–June 2022. *MMWR Morb Mortal Wkly Rep* **71**, (2022).
8. Freeman, D. *et al.* Injection fears and COVID-19 vaccine hesitancy. *Psychol Med* 1–11 doi:10.1017/S0033291721002609.
9. Kar, S. *et al.* Oral and intranasal vaccines against SARS-CoV-2: current progress, prospects, advantages, and challenges. *Immunity, Inflammation and Disease* **10**, e604 (2022).
10. Xu, H., Cai, L., Hufnagel, S. & Cui, Z. Intranasal vaccine: Factors to consider in research and development. *Int J Pharm* **609**, 121180 (2021).
11. Feng, L. *et al.* An adenovirus-vectored COVID-19 vaccine confers protection from SARS-COV-2 challenge in rhesus macaques. *Nat Commun* **11**, 4207 (2020).
12. Hassan, A. O. *et al.* A single-dose intranasal ChAd vaccine protects upper and lower respiratory tracts against SARS-CoV-2. *Cell* **183**, 169-184.e13 (2020).

13. Ku, M.-W. *et al.* Intranasal vaccination with a lentiviral vector protects against SARS-CoV-2 in preclinical animal models. *Cell Host Microbe* **29**, 236-249.e6 (2021).
14. van Doremalen, N. *et al.* Intranasal ChAdOx1 nCoV-19/AZD1222 vaccination reduces viral shedding after SARS-CoV-2 D614G challenge in preclinical models. *Science Translational Medicine* **13**, eabh0755 (2021).
15. Afkhami, S. *et al.* Respiratory mucosal delivery of next-generation COVID-19 vaccine provides robust protection against both ancestral and variant strains of SARS-CoV-2. *Cell* **185**, 896-915.e19 (2022).
16. Cokarić Brdovčak, M. *et al.* ChAdOx1-S adenoviral vector vaccine applied intranasally elicits superior mucosal immunity compared to the intramuscular route of vaccination. *European Journal of Immunology* **52**, 936–945 (2022).
17. Lei, H. *et al.* Intranasal administration of a recombinant RBD vaccine induces long-term immunity against Omicron-included SARS-CoV-2 variants. *Sig Transduct Target Ther* **7**, 1–13 (2022).
18. Wong, T. Y. *et al.* Intranasal administration of BReC-CoV-2 COVID-19 vaccine protects K18-hACE2 mice against lethal SARS-CoV-2 challenge. *NPJ Vaccines* **7**, 36 (2022).
19. An, X. *et al.* Single-dose intranasal vaccination elicits systemic and mucosal immunity against SARS-CoV-2. *iScience* **24**, 103037 (2021).
20. Li, X. F. *et al.* A highly immunogenic live-attenuated vaccine candidate prevents SARS-CoV-2 infection and transmission in hamsters. *Innovation (N Y)* 100221 (2022) doi:10.1016/j.xinn.2022.100221.
21. Ainai, A. *et al.* Intranasal vaccination with an inactivated whole influenza virus vaccine induces strong antibody responses in serum and nasal mucus of healthy adults. *Hum Vaccin Immunother* **9**, 1962–70 (2013).

22. Dhama, K. *et al.* COVID-19 intranasal vaccines: current progress, advantages, prospects, and challenges. *Human Vaccines & Immunotherapeutics* 1–11 (2022) doi:10.1080/21645515.2022.2045853.
23. Rice, A. *et al.* Heterologous saRNA Prime, DNA Dual-Antigen Boost SARS-CoV-2 Vaccination Elicits Robust Cellular Immunogenicity and Cross-Variant Neutralizing Antibodies. *Front Immunol* **13**, 910136 (2022).
24. Voigt, E. A. *et al.* A self-amplifying RNA vaccine against COVID-19 with long-term room-temperature stability. *npj Vaccines* **7**, 1–13 (2022).
25. Peng, Y. *et al.* Broad and strong memory CD4+ and CD8+ T cells induced by SARS-CoV-2 in UK convalescent individuals following COVID-19. *Nat Immunol* **21**, 1336–1345 (2020).
26. Rydyznski Moderbacher, C. *et al.* Antigen-specific adaptive immunity to SARS-COV-2 in acute COVID-19 and associations with age and disease severity. *Cell* **183**, 996-1012.e19 (2020).
27. Sui, Y. *et al.* An intranasally administrated SARS-CoV-2 beta variant subunit booster vaccine prevents beta variant replication in rhesus macaques. *PNAS Nexus* **1**, pgac091 (2022).
28. McKay, P. F. *et al.* Self-amplifying RNA SARS-CoV-2 lipid nanoparticle vaccine candidate induces high neutralizing antibody titers in mice. *Nat Commun* **11**, 3523 (2020).
29. de Alwis, R. *et al.* A single dose of self-transcribing and replicating RNA-based SARS-CoV-2 vaccine produces protective adaptive immunity in mice. *Mol Ther* **29**, 1970–1983 (2021).
30. Gerhardt, A. *et al.* A flexible, thermostable nanostructured lipid carrier platform for RNA vaccine delivery. *Mol Ther Methods Clin Dev* **25**, 205–214 (2022).
31. McMahan, K. *et al.* Correlates of protection against SARS-CoV-2 in rhesus macaques. *Nature* **590**, 630–634 (2021).
32. Gilbert, P. B. *et al.* Immune correlates analysis of the mRNA-1273 COVID-19 vaccine efficacy clinical trial. *Science* **375**, 43–50 (2022).

33. Graham, B. S. Rapid COVID-19 vaccine development. *Science* **368**, 945–946 (2020).

34. Weiskopf, D. *et al.* Phenotype and kinetics of SARS-CoV-2-specific T cells in COVID-19 patients with acute respiratory distress syndrome. *Sci Immunol* **5**, eabd2071 (2020).

35. Jackson, L. A. *et al.* An mRNA vaccine against SARS-CoV-2 - preliminary report. *N Engl J Med* **383**, 1920–1931 (2020).

36. Lurie, N., Saville, M., Hatchett, R. & Halton, J. Developing Covid-19 vaccines at pandemic speed. *N Engl J Med* **382**, 1969–1973 (2020).

37. Yuan, R. *et al.* The roles of tissue-resident memory T cells in lung diseases. *Frontiers in Immunology* **12**, 710375 (2021).

38. Elgueta, R. *et al.* Molecular mechanism and function of CD40/CD40L engagement in the immune system. *Immunol Rev* **229**, 10.1111/j.1600-065X.2009.00782.x (2009).

39. Mikhak, Z., Strassner, J. P. & Luster, A. D. Lung dendritic cells imprint T cell lung homing and promote lung immunity through the chemokine receptor CCR4. *J Exp Med* **210**, 1855–1869 (2013).

40. Lim, J. M. E. *et al.* SARS-CoV-2 breakthrough infection in vaccinees induces virus-specific nasal-resident CD8+ and CD4+ T cells of broad specificity. *J Exp Med* **219**, e20220780 (2022).

41. Park, Y.-J. *et al.* Imprinted antibody responses against SARS-CoV-2 Omicron sublineages. *bioRxiv* 2022.05.08.491108 (2022) doi:10.1101/2022.05.08.491108.

42. Tang, J. *et al.* Respiratory mucosal immunity against SARS-CoV-2 following mRNA vaccination. *Science Immunology* **0**, eadd4853 (2022).

43. Polack, F. P. *et al.* Safety and efficacy of the BNT162b2 mRNA Covid-19 vaccine. *N Engl J Med* **383**, 2603–2615 (2020).

44. Baden, L. R. *et al.* Efficacy and safety of the mRNA-1273 SARS-CoV-2 vaccine. *N Engl J Med* **384**, 403–416 (2021).

45. El Sahly, H. M. *et al.* Efficacy of the mRNA-1273 SARS-CoV-2 vaccine at completion of blinded phase. *N Engl J Med* **385**, 1774–1785 (2021).

46. Watson, O. J. *et al.* Global impact of the first year of COVID-19 vaccination: a mathematical modelling study. *The Lancet Infectious Diseases* **0**, (2022).

47. Giannotta, G. & Giannotta, N. mRNA COVID-19 vaccines and long-lived plasma cells: a complicated relationship. *Vaccines (Basel)* **9**, 1503 (2021).

48. Ibarrondo, F. J. *et al.* Primary, recall, and decay kinetics of SARS-CoV-2 vaccine antibody responses. *ACS Nano* **15**, 11180–11191 (2021).

49. Keehner, J. *et al.* Resurgence of SARS-CoV-2 infection in a highly vaccinated health system workforce. *N Engl J Med* **385**, 1330–1332 (2021).

50. Menni, C. *et al.* COVID-19 vaccine waning and effectiveness and side-effects of boosters: a prospective community study from the ZOE COVID Study. *The Lancet Infectious Diseases* **22**, 1002–1010 (2022).

51. Rele, S. COVID-19 vaccine development during pandemic: gap analysis, opportunities, and impact on future emerging infectious disease development strategies. *Hum Vaccin Immunother* **17**, 1122–1127 (2021).

52. Ren, X. *et al.* Reinfection in patients with COVID-19: a systematic review. *Glob Health Res Policy* **7**, 12 (2022).

53. Araf, Y. *et al.* Omicron variant of SARS-CoV-2: Genomics, transmissibility, and responses to current COVID-19 vaccines. *J Med Virol* **94**, 1825–1832 (2022).

54. Cevik, M., Grubaugh, N. D., Iwasaki, A. & Openshaw, P. COVID-19 vaccines: Keeping pace with SARS-CoV-2 variants. *Cell* **184**, 5077–5081 (2021).

55. Maher, M. C. *et al.* Predicting the mutational drivers of future SARS-CoV-2 variants of concern. *Science Translational Medicine* **14**, eabk3445 (2022).

56. Wright, P. F. *et al.* Longitudinal Systemic and Mucosal Immune Responses to SARS-CoV-2 Infection. *The Journal of Infectious Diseases* jiac065 (2022) doi:10.1093/infdis/jiac065.

57. Alu, A. *et al.* Intranasal COVID-19 vaccines: From bench to bed. *EBioMedicine* **76**, 103841 (2022).

58. Mudrick, H. E. *et al.* Comparison of Mucosal and Intramuscular Immunization against SARS-CoV-2 with Replication-Defective and Replicating Single-cycle Adenovirus Vaccines. 2021.04.20.440651 Preprint at https://doi.org/10.1101/2021.04.20.440651 (2021).

59. Corbett, K. S. *et al.* SARS-CoV-2 mRNA vaccine design enabled by prototype pathogen preparedness. *Nature* **586**, 567–571 (2020).

60. Naaber, P. *et al.* Dynamics of antibody response to BNT162b2 vaccine after six months: a longitudinal prospective study. *The Lancet Regional Health - Europe* **10**, 100208 (2021).

61. Carter, N. J. & Curran, M. P. Live attenuated influenza vaccine (FluMist®; Fluenz™): a review of its use in the prevention of seasonal influenza in children and adults. *Drugs* **71**, 1591–1622 (2011).

62. Banihashemi, S. R. *et al.* Safety and Efficacy of Combined Intramuscular/Intranasal RAZI-COV PARS Vaccine Candidate Against SARS-CoV-2: A Preclinical Study in Several Animal Models. *Front Immunol* **13**, 836745 (2022).

63. Waltz, E. China and India approve nasal COVID vaccines — are they a game changer? *Nature* **609**, 450–450 (2022).

64. Xu, F. *et al.* Safety, mucosal and systemic immunopotency of an aerosolized adenovirus-vectored vaccine against SARS-CoV-2 in rhesus macaques. *Emerging Microbes & Infections* **11**, 439–442 (2022).

65. Slütter, B., Pewe, L. L., Kaech, S. M. & Harty, J. T. Lung Airway-Surveilling CXCR3hi Memory CD8+ T Cells Are Critical for Protection against Influenza A Virus. *Immunity* **39**, 939–948 (2013).

66. Rice, A. *et al.* Intranasal plus subcutaneous prime vaccination with a dual antigen COVID-19 vaccine elicits T-cell and antibody responses in mice. *Sci Rep* **11**, 14917 (2021).

67. Wong, T. Y. *et al.* Intranasal administration of BReC-CoV-2 COVID-19 vaccine protects K18-hACE2 mice against lethal SARS-CoV-2 challenge. *NPJ Vaccines* **7**, 36 (2022).
68. Mao, T. *et al.* Unadjuvanted intranasal spike vaccine booster elicits robust protective mucosal immunity against sarbecoviruses. *bioRxiv* 2022.01.24.477597 (2022) doi:10.1101/2022.01.24.477597.
69. ImmunityBio, Inc. *THEMBA II T-CELL Vaccine: A Phase 1/2 Study of the Safety, Reactogenicity, and Immunogenicity of Vaccination With saRNA COVID-19 Vaccines*. https://clinicaltrials.gov/ct2/show/NCT05370040 (2022).
70. Son, Y. M. *et al.* Tissue-resident CD4+ T helper cells assist the development of protective respiratory B and CD8+ T cell memory responses. *Sci Immunol* **6**, eabb6852 (2021).
71. Swarnalekha, N. *et al.* T resident helper cells promote humoral responses in the lung. *Sci Immunol* **6**, eabb6808 (2021).
72. Erasmus, J. H. *et al.* A Nanostructured Lipid Carrier for Delivery of a Replicating Viral RNA Provides Single, Low-Dose Protection against Zika. *Mol Ther* **26**, 2507–2522 (2018).
73. Committee for the Update of the Guide for the Care and Use of Laboratory Animals. *Guide for the Care and Use of Laboratory Animals*. (The National Academies Press, 2011).
74. Crawford, K. H. D. *et al.* Protocol and reagents for pseudotyping lentiviral particles with SARS-CoV-2 spike protein for neutralization assays. *Viruses* **12**, 513 (2020).